Received: 10 May 2020 | Revised: 8 August 2020 | Accepted: 13 August 2020

DOI: 10.1002/eqe.3345

RESEARCH ARTICLE

WILEY

Torsional ductility spectrum for predicting ductility distribution in simple asymmetric-plan structures

Halûk Sucuoğlu[1] | **Kaan Kaatsız**[2]

[1]Department of Civil Engineering, Middle East Technical University, Ankara, Turkey

[2]Department of Civil Engineering, Ahi Evran University, Kırşehir, Turkey

Correspondence
Halûk Sucuoğlu, Department of Civil Engineering, Middle East Technical University, 06880 Ankara, Turkey.
Email: sucuoglu@metu.edu.tr

Summary

An analytical procedure is developed for predicting the ductility demands in simple asymmetric-plan structures under earthquake ground motions. The procedure governs regular structures dominated by the lower vibration modes where inelastic response occurs only at the bases of first story columns and at the beam ends, in conformance with the capacity design principles. *Torsional ductility spectra* are generated for expressing the maximum ductility response of torsionally coupled, generic, single-story, 2-degree-of-freedom inelastic parametric systems. Five parameters characterize the parametric systems: first mode period, uncoupled frequency ratio, stiffness eccentricity, stiff-to-flexible edge strength ratio, and ductility reduction factor. A surrogate modeling approach is developed for converting the properties of the actual systems to those of the parametric system. Mean maximum ductilities of torsionally stiff, equally stiff, and torsionally flexible systems are calculated under a set of design spectrum compatible strong motions for the possible combinations of characteristic parameters. The results obtained from case studies revealed reasonable accuracy of the estimations. The results have indicated that the flexible side frames of torsionally stiff and equally stiff code conforming designs are mainly responsible for providing the intended ductility and energy dissipation capacity whereas the stiff side frames play a secondary role, particularly when the stiff edge is significantly stronger than the flexible edge. However, ductility demands in torsionally flexible systems are significantly larger at both sides compared with torsionally stiff systems.

KEYWORDS

asymmetric-plan structures, ductility distribution, performance assessment, torsional coupling, torsional ductility spectra, uniform ductility spectra

1 | INTRODUCTION

Conventional seismic design is based on controlling the inelastic response of structures under strong ground motions by employing linear elastic analysis procedures. Such an approach is inevitable because inelastic response analysis cannot be performed before completing design, yet it is far from being practical. Modern seismic design codes have introduced response reduction factors for estimating the design forces of structural members from the results of linear elastic analysis.[1,2] Although this approach leads to acceptable seismic performances for regular structures when

capacity design principles are implemented in design, it is usually not be the case for asymmetric-plan structures subjected to significant torsional coupling under strong ground motions.

Earlier research work on investigating the adequacy of code procedures in controlling inelastic seismic response was based on single-story inelastic shear frame models.[3] Although these models oversimplify the actual inelastic seismic behavior of asymmetrical multistory frame structures,[4] a systematic evaluation of the large number of system parameters that are in complex interaction during seismic response cannot be possible otherwise. The basic aim of these studies were suggesting improvements to linear elastic code procedures in order to achieve a balanced distribution of inelastic deformations, either by proposing a design eccentricity or by imposing an uneven distribution of response reduction factors at the stiff and flexible sides. Their crucial findings and design implications are summarized below.

Erdik[5] and Kan and Chopra[6] were among the first researchers to observe diminishing effects of torsional coupling with increasing inelastic deformations. Chandler and Hutchinson[7] introduced an effective eccentricity and an associated design torque. Upon its implementation in design, elastic edge displacements obtained from linear elastic analysis matches those of inelastic dynamic analysis reasonably well. However, the procedure leads to overly conservative design in certain ranges of uncoupled torsional–translational frequency ratio. Tso and Bozorgnia[8] similarly introduced an effective eccentricity expression in terms of static eccentricity and uncoupled frequency ratio for estimating the inelastic dynamic edge displacements. Hence, ductility demands of the inelastic system can be directly predicted from the results of linear elastic analysis, and design can be revised if necessary. Rutenberg et al.[9,10] observed that peak ductility demands at the edges of asymmetric-plan systems are not necessarily larger than those of companion symmetric systems and can be reduced by adjusting the strength distribution. They explored the influence of the center of strength (CV) location on peak ductility demand by locating CV at the center of mass (CM), at the center of stiffness (CR), or halfway between CM and CR. Halfway location is identified as most efficient for reducing peak ductility demand. Goel and Chopra[11,12] and Chandler and Duan[13] also identified strength eccentricity as the more effective parameter compared with stiffness eccentricity. Strength-symmetric systems are affected less from stiffness asymmetry compared with the strength asymmetric systems under strong earthquake excitations. They have further recommended that a torsionally coupled system designed for ultimate limit state may not remain elastic under service-level earthquake excitations. Therefore, buildings have to be designed to satisfy both limit states separately. Either one of the limit states may govern the lateral strength of a frame.

Correnza et al.[14] investigated code torsional provisions in terms of deformation and ductility demands. According to their findings, allowing strength reduction at the stiff side makes these members more critical in ductility demands than the flexible side members. Hence, strength reduction is not suggested at the stiff edge. Paulay[15] proposed a displacement-based design approach as an alternative to the conventional strength based approach. A relation between system ductility, assigned at the CM, and ductility capacity of the most critical member is obtained from displacement geometry. Accordingly, strength reduction in design is limited to the calculated system ductility. Humar and Kumar[16] defined separate effective design eccentricities for the flexible and stiff sides of the linear elastic single-story systems in terms of static eccentricity and torsional frequency ratio. Separate effective lateral load analysis with these eccentricities would produce maximum displacements similar to those obtained from response spectrum analysis under idealized design spectra. When compared with the design eccentricities in the codes, design strengths obtained with the proposed pair of eccentricities reduced overdesign of the code procedures, particularly for the flexible side. Inelastic response analysis indicated reasonable conservatism for the flexible side when the system is torsionally stiff. Myslimaj and Tso[17] proposed a balanced center of strength and center of stiffness in order to minimize the edge displacements of torsionally coupled systems. When CV is located with the same eccentricity as CR, but on the opposite side of CM, inelastic torsional response reduces significantly under earthquake ground motions. Paulay[18] and Humar and Kumar[19] considered the contribution of orthogonal frames to torsional response in single-story models under uniaxial excitation. Kaatsız and Sucuoğlu[20] derived uniform ductility spectra that provides optimum strength ratio of stiff side to flexible side for achieving balanced ductility demands at the stiff and flexible sides of the plan under strong earthquake excitations.

The survey presented here on single-story inelastic asymmetric systems admittedly does not cover the entire literature. Rutenberg,[3,21] De Stefano and Pintucchi,[22] and Anagnostopoulos et al.[23] published comprehensive reviews on this broad topic. There is a common agreement, however, in most of the conducted research, that strength eccentricity is more effective compared with the stiffness eccentricity in controlling inelastic torsional response. Assigning different eccentricities at stiff and flexible sides through accidental eccentricity formulations in seismic code approaches does not usually compensate the uneven distribution of inelastic deformation demands,[16,24] but rather increase overstrength. An optimal strength eccentricity may lead to a more uniform inelastic deformation distribution regardless of the stiffness eccentricity despite interdependance of strength and stiffness.

Implementation of design suggestions obtained from single-story inelastic shear frame models to multistory frame structures is not straight forward due to several reasons: Seismic response of asymmetric-plan multistory frames are far complex compared with single-story shear frames due to higher mode effects and vertical irregularities. Moreover, stiffness eccentricity and uncoupled frequency ratio cannot be defined analytically for multistory moment frames. Accordingly, torsion researchers focused their attention on investigating the seismic response of asymmetric multistory frames rather than transforming the results obtained from single-story models.

Duan and Chandler[25] extended torsional response studies to the inelastic seismic response of code-designed multistory frame structures. For the multistory building models that they employed with regular asymmetry, the results obtained from single-story unsymmetrical systems were mostly consistent. They observed higher ductility demands at the stiff side members whereas the deformation demands from flexible side members were higher. Accordingly, seismic provisions that do not allow strength reduction at the stiff side were favored. They developed design charts for obtaining similar ductility demands at the flexible and stiff side members. De la Llera and Chopra[26] studied a five-story shear-type building frame with plan-wise and height-wise irregularities and investigated the effects of stiffness and strength asymmetry, strength of orthogonal planes, and bidirectional ground motions on the inelastic torsional response. They have also observed convincing similarities between the responses of single-story parametric systems and the actual multistory shear frames; hence, the results obtained from single-story inelastic models may be largely applicable to the inelastic seismic response of multistory frames. Stiffness eccentricity influences elastic response more, but strength eccentricity controls inelastic response. Increasing torsional strength of stories does not necessarily help reducing torsional response but provides more uniform distribution of strength among resisting planes. Similar to previous results obtained from single-story models, bringing the center of strength as close as possible to the center of mass at each story leads to a more balanced inelastic deformation distribution among the resisting frames. When the intensity of ground motion in the orthogonal direction is large enough to cause yielding in the orthogonal frames, then their contribution to a uniform distribution of inelastic deformation demands has to be ignored. They have finally suggested a design approach based on modifying the story shear–story torque surface for achieving a more uniform inelastic deformation demand distribution on the resisting planes. More recently, Lee and Hwang[27] conducted one of the few shaking table tests on unsymmetrical-plan test frames. Their test results have demonstrated the erratic variation of instantaneous stiffness eccentricity, with peak values decreasing as ground motion intensity increases. Hence, stiffness eccentricity should not represent the actual torsional behavior as a design parameter. They suggested employing story shear–story torque capacity diagrams as a design tool instead of using stiffness eccentricity as a design parameter, in support of De la Llera and Chopra.[26] A design methodology has not been proposed however. Marusic and Fajfar[28] investigated the inelastic seismic response of multistory frames under biaxial ground motions. They reached a conclusion confirming the diminishing effect of torsional coupling with higher levels of nonlinearity in the system.

Stathopoulos and Anagnostopoulos[29] tested the design objectives of major seismic design codes, namely, UBC and Eurocode, based on three-dimensional multistory building models with biaxial eccentricity, excited by a set of two-component earthquake motions. They observed that code-designed structures do not exhibit a balanced ductility distribution during inelastic time history analysis. Ductilities of the flexible side members usually exceed those of the stiff side, although single-story models predict the opposite. Hence, radical changes are required for improving seismic codes. Kyrkos and Anagnostopoulos[30,31] have in turn suggested a two-stage design procedure where the top story displacements of the flexible and stiff edges are obtained at the first stage. Then, modification factors for both edges are computed from the edge displacements and applied to the member design forces. Flexible edge factor always increases, and the stiff edge factor reduces the associated member sizes. It has been shown on several case studies that the modified design leads to a more balanced distribution of inelastic displacements along the building height compared with the original design.

De Stefano et al.[32] studied the uneven distribution of overstrength in torsionally coupled multistory buildings, which affects the distribution of yielding significantly. They suggested explicit consideration of overstrength distribution in design. Ghersi et al.[33] proposed a design procedure that requires a two-level analysis. Standard modal analysis is carried out first. Then, a design eccentricity is defined which requires moving the mass center toward the stiffness center, and then, the second analysis is carried out. Hence, favorable but unrealistic effect of deck rotation in reducing the stiff side displacements during linear elastic response is prevented. Such a favorable effect is not observed when inelastic response is significant, as mentioned above. This second analysis can be performed by constraining the deck rotations as well, which is simpler in implementation.

Kosmopoulos and Fardis[34] calculated the chord rotations of existing asymmetric buildings both from inelastic response history analysis under a set of ground motions compatible with the code spectrum and from response

spectrum analysis. They observed that standard response spectrum analysis overestimates chord rotations when torsional effects are significant. Therefore, the conservatism of linear elastic design procedures should be considered in design for achieving more realistic performance objectives. Bahmani et al.[35] extended the direct displacement design procedure, originally developed for plane frames, to unsymmetrical-plan space frames. This procedure requires additional analysis for decoupling translational and rotational displacements. Case studies are presented to verify that the targeted interstory drifts are achieved during inelastic seismic response under design-level ground motions.

Although disparities exist in implementation, a common agreement in the studies reviewed here is reducing strength eccentricity for achieving an acceptable inelastic torsional response. This usually leads toward a more symmetrical system due to strength–stiffness dependence, which contradicts however with the inherent causes of torsion.

Despite numerous suggestions from the huge mass of research conducted in the past, classical seismic design procedures for unsymmetrical-plan buildings did not go through significant changes in seismic design codes during the last decades. The only particular requirement pertaining to torsion in seismic design is introducing accidental eccentricity and discouraging excessive rotational flexibility.[1,2]

1.1 | Simple realities about seismic torsion

The main causes of torsion are the requirements imposed by architectural design, as well as gravity and service design requirements that are somehow interrelated. These requirements lead to a preliminary design where the architect essentially sets the locations and dimensions of structural members. Structural engineer has limited control over these parameters unless they challenge basic structural safety. In fact, all building structures are unsymmetrical to a certain extent without exception. Perfect symmetry in structural plan cannot usually be achieved due to the constraints in land use, different service requirements of enclosed spaces within the building as well as facades at the exterior. Therefore, structural engineer has to deal with all these issues in distributing stiffness and strength among vertical members.

One particular issue regarding code-based structural design is crucial. When the lateral stiffnesses of exterior frames on opposite sides are significantly different, which indeed is the main cause of stiffness eccentricity, the current force-based design procedure demands less strength from the stiff side frame and more from the flexible side frame. This is schematized in Figure 1 for a one-story, torsionally stiff parametric shear frame composed of two lateral load-resisting members. The stiff and flexible side frame displacements u_S and u_F, and the associated design strength demands F_S and F_F are determined through modal response spectrum analysis. Design strength demands always satisfy (F_F F_S) at all periods in a stiffness eccentric system under a typical code spectrum when $e < 0.25$. This is however contrasting the reality due to inherent overstrength of the stiff side, resulting from strength–stiffness proportionality. Although a nominal design for the flexible side frames may be achieved with reasonable overstrength, the actual existing strength of the stiff side frames dictated by "larger than necessary" member dimensions, material design strengths, and detailing requirements shall always be much larger than the design strength demand. Hence, a significant, excessive overstrength at the stiff side proportional to its stiffness is always present inevitably. The effect of stiff side overstrength on the inelastic seismic response of asymmetric-plan systems was comprehensively discussed in Kaatsız and Sucuoğlu.[20]

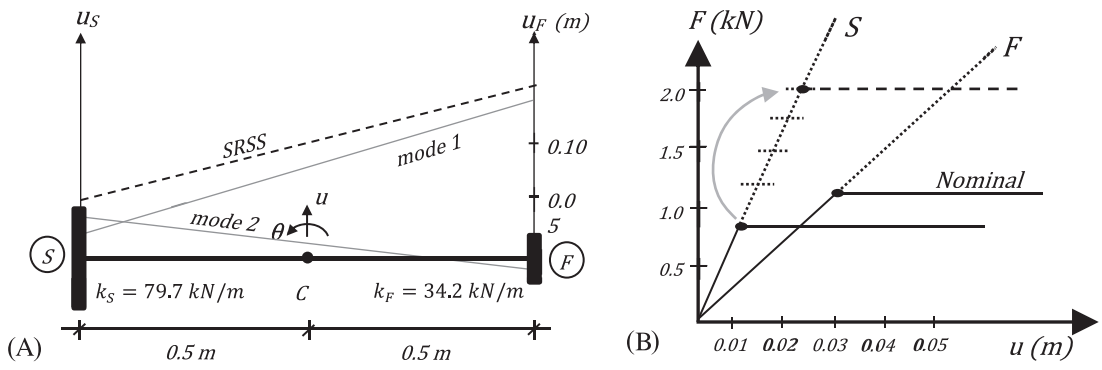

FIGURE 1 A, Schematic distribution of displacements for a 2DOF parametric system (ω_1=9 r/s, ω_2=14.5 r/s, L = 1 m, m = 1 ton, Ω_r = 1.25) and B, design strength demands (R_μ = 4) and stiff side overstrength variation

Because the design engineer has very limited control in assigning an intended strength to the stiff side frame for achieving a balanced ductility distribution, it is prudent to revise such a wishful performance objective. A more realistic design approach would be accepting lower ductility performance from the stiff side due to lower demand, while supplying the required ductility capacity to the flexible side for acceptable seismic performance. Accidental eccentricity introduced in seismic codes only increases the design strengths of both sides, which introduces further overstrength to the stiff side frames. Hence, its effectiveness in providing a balanced inelastic deformation distribution along lateral load-resisting members in plan is not warranted, as previously discussed by Humar and Kumar[16] and Stathopoulos and Anagnostopoulos.[24]

1.2 | Research objective

Basic research objective is estimating the ductility demands at the first story columns in simple asymmetric-plan MDOF structures under design-level strong motion excitations, by introducing a simple spectral tool. The spectral tool is the torsional ductility spectra (TDSs), which is developed in terms of the basic vibration and strength parameters of the simplest single-story, 2DOF asymmetric shear frame. The final task is introducing a practical procedure for implementing TDSs to the inelastic seismic response of actual, code-designed, regular multistory building structures with plan asymmetry.

2 | TORSIONAL DUCTILITY SPECTRA

TDS is a graphical tool developed in this study for predicting the stiff and flexible side ductilities of a single-story shear frame with one way asymmetry under design-level ground motions. The shear frame is composed of a stiff side and a flexible side vertical member, connected to a uniform rigid slab.

A large set of single-story parametric shear frame models with a flexible and a stiff side member are designed under a typical design spectrum representing strong ground shaking at the near fault region of a major causative fault. Design spectrum is reduced by the ductility reduction factor R_μ that takes values of 3, 4, 5, and 6. Three different stiffness eccentricity ratios $e = 0.1$, 0.2, and 0.3 are considered. The 2DOF parametric system, schematized in Figure 1A for a particular case, has a uniform mass m of 1 ton and its length L is 1 m.

For the linear elastic system, stiff and flexible side stiffnesses k_S and k_F are selected such that their sum and difference (or product) satisfy a target e value and a target first mode frequency ω_1. Mass moment of inertia I_{CM} is determined from the selected uncoupled frequency ratio $\Omega_r = \omega_\theta/\omega_y$, which is taken as 1.25 for a torsionally stiff system, 1.0 for a torsionally equally stiff system and 0.8 for a torsionally flexible system.

The relationship between modal vibration frequency ω_n, stiffnesses k_S and k_F, and the inertial properties m and I_{CM} of the parametric system in Figure 1A can be obtained from the solution of the eigenvalue problem,

$$\det\left(\underline{k} - \omega_n^2 \underline{m}\right) = 0, \tag{1}$$

where

$$\underline{k} = \begin{bmatrix} (k_S + k_F) & (-k_S + k_F)\dfrac{L}{2} \\ (-k_S + k_F)\dfrac{L}{2} & (k_S + k_F)\dfrac{L^2}{4} \end{bmatrix}; \underline{m} = \begin{bmatrix} m & 0 \\ 0 & mr^2 \end{bmatrix}; r^2 = \frac{I_{CM}}{m}. \tag{2}$$

The solution of Equation 1, combined with Equation 2, leads to the characteristic equation

$$(mr)^2 \omega_n^4 - m(k_S + k_F)\left(r^2 + \frac{L^2}{4}\right)\omega_n^2 + (k_S \cdot k_F)L^2 = 0; n = 1, 2. \tag{3}$$

r is the radius of gyration in the above equation, which is directly related to the uncoupled frequency ratio Ω_r through

$$\Omega_r = \frac{L}{2r}. \tag{4}$$

Introducing r from Equation 4 for the uncoupled frequency ratio, $m = 1$ and $L = 1$ for the parametric system, Equation 3 provides one equation for the two unknowns k_S and k_F for a given ω_1 (or T_1). The second equation comes from the stiffness eccentricity definition:

$$e = \frac{k_F - k_S}{2(k_F + k_S)}. \tag{5}$$

Accordingly, k_S and k_F corresponding to T_1 for the six combinations of $e = 0.1$, 0.2, or 0.3 and $\Omega_r = 1.25$, 1.0, or 0.8 are calculated by solving Equations 3 and 5 simultaneously.

After determining the linear elastic properties of each parametric system, they are designed under the response spectrum shown in Figure 2A for obtaining the stiff side and flexible side strength demands for selected ductility reduction factors of $R_\mu = 3$, 4, and 5. S_S and S_1 are the mapped short period and 1-s spectral accelerations, whereas S_{MS}, S_{M1} and S_{DS}, S_{M1} pairs are the spectral accelerations at the same periods for maximum and design-level earthquake intensities. F_a and F_v are the site factors, and T_0 and T_S are the corner periods of the spectrum described per ASCE 7-16. Accidental eccentricity is not considered in design. The flexible side nominal strength is held fixed whereas overstrength is introduced to the stiff side members incrementally as shown in Figure 1B for generating a realistic family of parametric systems represented by their stiff to flexible side strength ratios (*SFSR*s), where

$$SFSR = \frac{F_S}{F_F}. \tag{6}$$

Finally, nonlinear dynamic response of each parametric system, identified with the parameters (T_1, Ω_r, e, R_μ, and *SFSR*) are computed under a set of 30 spectrum-matched ground motions selected from PEER NGA Database.[36] Spectrum matching[37] is preferred here as the scaling method because the same set of scaled ground motions has to be employed for all parametric systems with different modal vibration periods. The list of 30 unscaled ground motions and their basic seismological characteristics are presented in Appendix A. They are all recorded on soft soil, at near fault regions with Joyner–Boore distances less than 40 km, during earthquakes with magnitudes between 6.0 and 7.5. Nonlinear models of the 2DOF parametric systems are prepared in the OpenSees[38] platform, where elastic-perfectly plastic hysteresis models are employed.

The results of nonlinear dynamic response analyses are compiled in the form of Torsional ductility spectra. Mean maximum ductility is utilized as the inelastic response parameter because it is a normalized value that provides an objective response comparison for all parametric systems considered herein. Torsional ductility spectra produced for

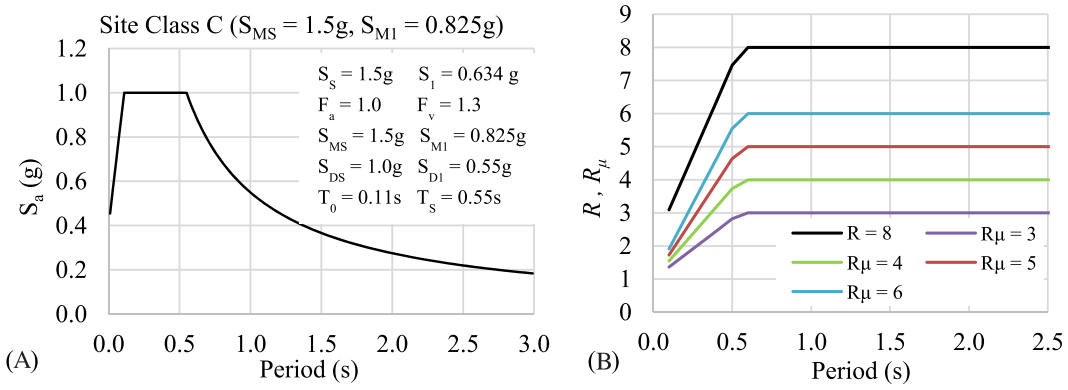

FIGURE 2 A, Design spectrum and B, response reduction factor [Colour figure can be viewed at wileyonlinelibrary.com]

R_μ = 3, 4, and 5 are presented in Figures 3, 4, and 6, respectively. Only the results obtained for torsionally stiff and equally stiff systems (Ω_r = 1.25 and 1.0) are presented in these figures because including the results of torsionally flexible systems makes the graphical view quite complicated. Torsionally flexible systems are discussed comparatively in a separate section.

The accompanying *uniform ductility spectra* for the same ductility reduction factors, developed recently by Kaatsız and Sucuoğlu,[20] are also given in Figures 5 and 7 for R_μ = 4 and 5. Uniform ductility spectrum is another practical spectral tool that was developed for the similar 2DOF parametric systems and ground motions that are employed to derive the TDSs introduced herein. These spectra simply provide the optimal *SFSR* values (Equation 6) in order to attain equal ductility ratios at the stiff and flexible sides of the single-story shear frames under design spectrum compatible ground motions. In these graphs, the ratio of stiff side to flexible side strengths is expressed by *SFSR*. Nominal or design strength curve is the ratio of strength demands obtained directly from code design, as shown in Figure 1A. It is noteworthy that the optimal strength ratios leading to equal ductilities of both sides are always running above the nominal curves in uniform ductility spectra. They were obtained by varying the stiff side strengths, as shown in Figure 2B, which was discussed previously. This observation is implying that uniform ductility distribution can never be achieved in a code-designed unsymmetrical-plan system. Pairwise presentation of torsional and uniform ductility spectra in Figures 4–7 facilitates comparative discussions.

2.1 | Basic observations on torsional ductility spectra

The most notable observation is on the differences of ductilities at the stiff and flexible side members. Flexible side ductilities are almost equal to R_μ regardless of *SFSR* and stiffness eccentricity. They only reduce slightly at short periods where R_μ is also reduced (Figure 2B). Stiff side ductilities however are quite sensitive to *SFSR*. As *SFSR* approaches the optimal value indicated by *uniform ductility spectra* at a given period (Figures 3, 4, and 6), ductility of the stiff side also approaches R_μ. Note here again that *SFSR* variation corresponds to the proportional variation of stiff side strength

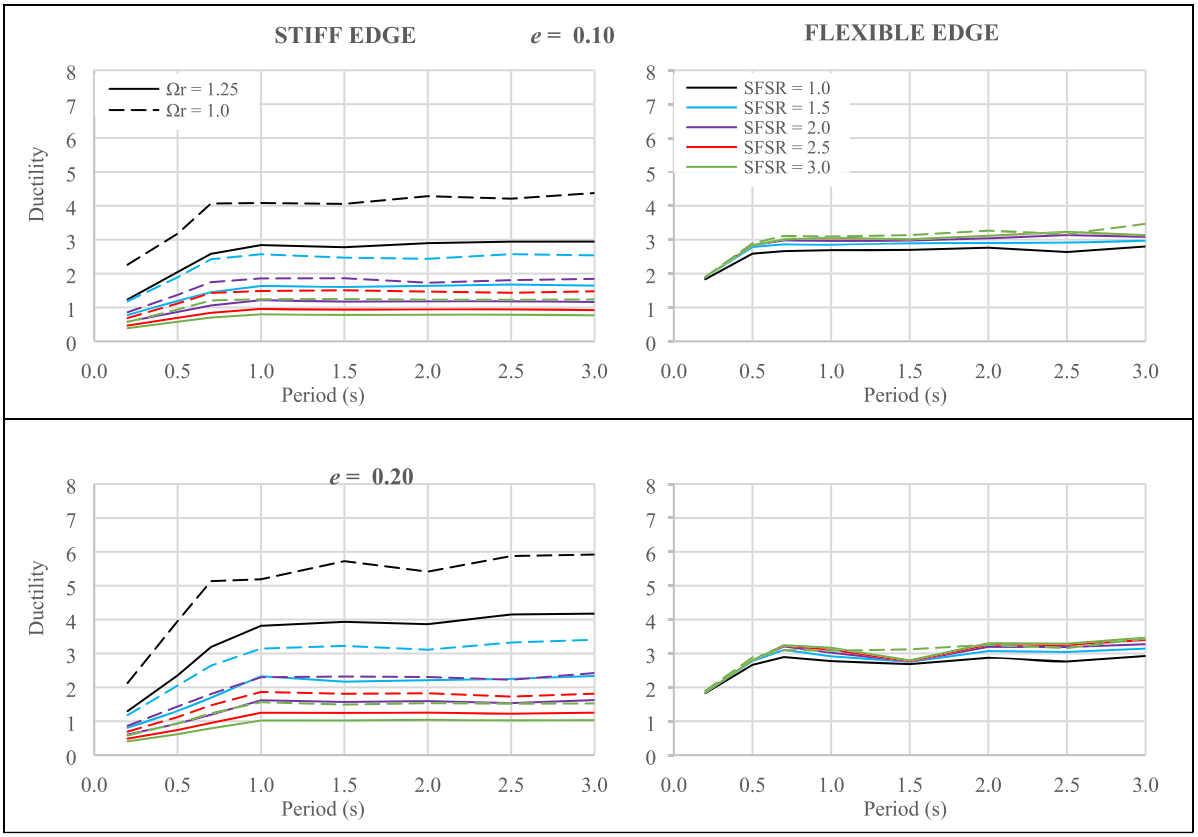

FIGURE 3 Torsional ductility spectra (R_μ = 3) [Colour figure can be viewed at wileyonlinelibrary.com]

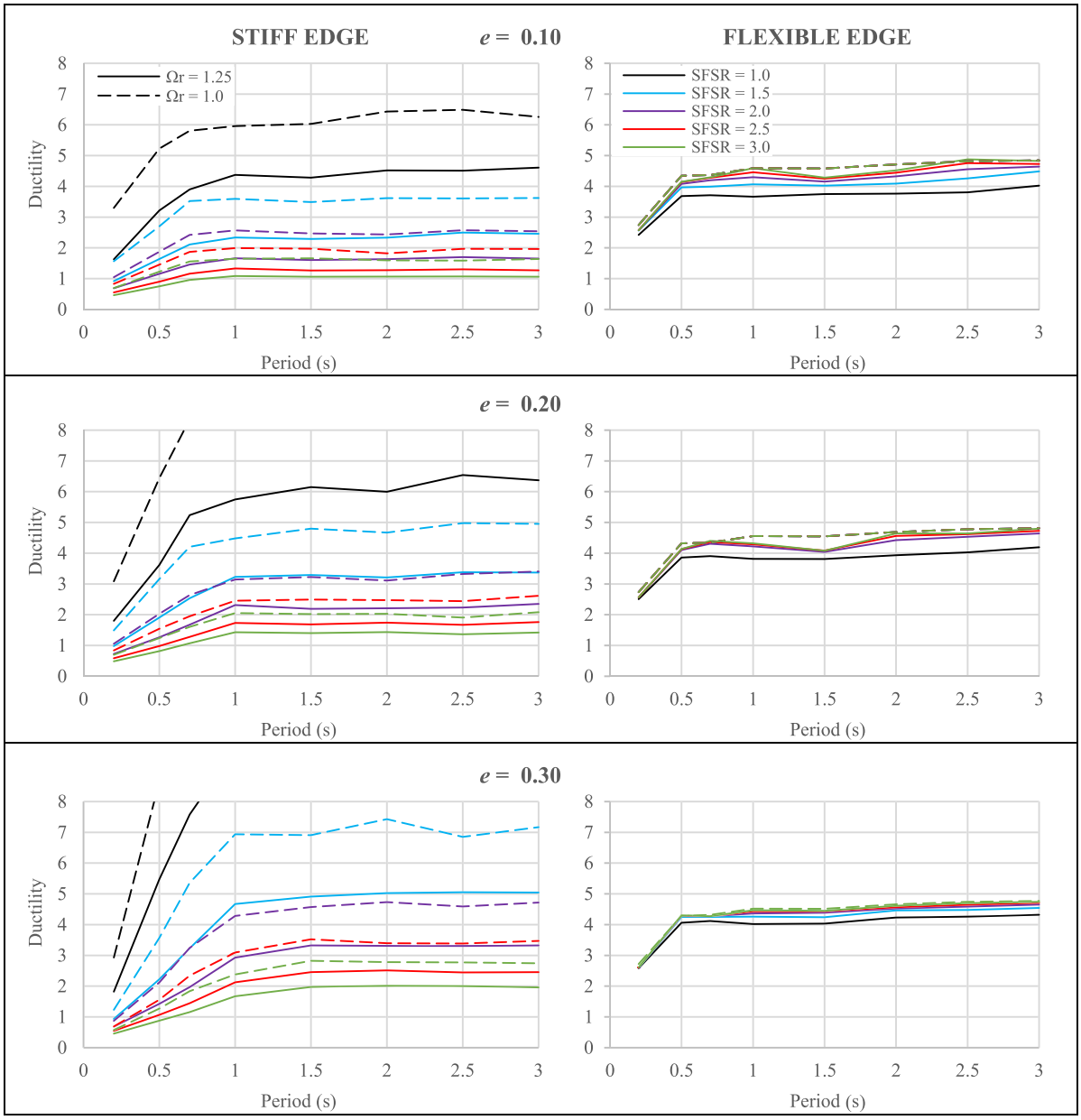

FIGURE 4 Torsional ductility spectra ($R_\mu = 4$) [Colour figure can be viewed at wileyonlinelibrary.com]

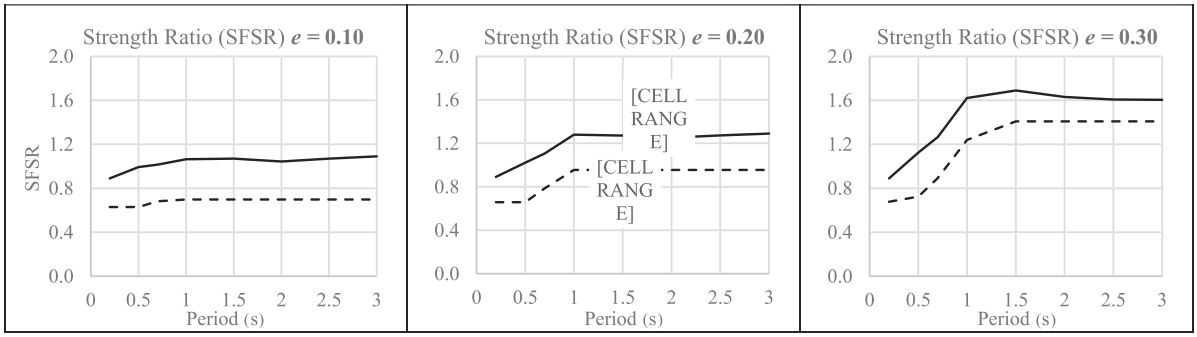

FIGURE 5 Uniform ductility spectra ($R_\mu = 4$)

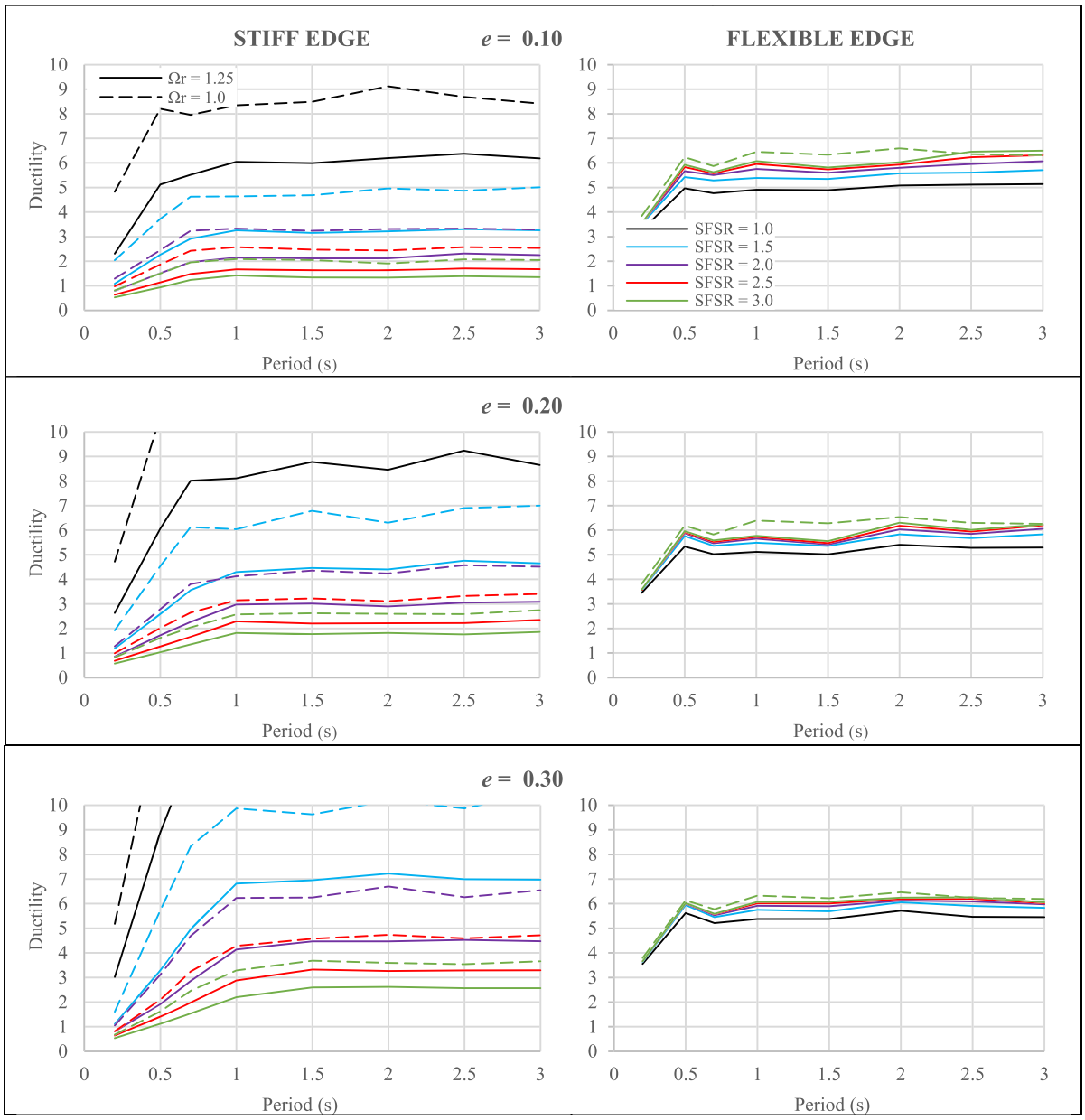

FIGURE 6 Torsional ductility spectra ($R_\mu = 5$) [Colour figure can be viewed at wileyonlinelibrary.com]

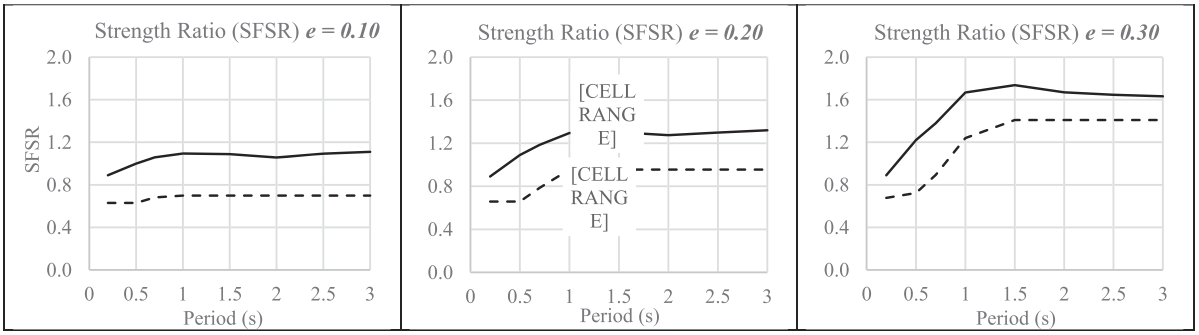

FIGURE 7 Uniform ductility spectra ($R_\mu = 5$)

(Figure 1B) because the flexible side strength is held fixed at its nominal design value. But because this optimal value is always larger than the nominal, reduction of *SFSR* toward nominal leads to very high ductility demands at the stiff side (see $SFSR = 1.0$ curves in Figures 3, 4, and 6 for $e = 0.2$ and 0.3). Correnza et al.[14] discussed this phenomenon previously where they suggested no strength reduction at the stiff edge due to expected ductile response. In fact, inelastic response develops at the stiff side under strong excitations, although at a much lesser level compared with the flexible side depending on its inherent overstrength.

This observation leads to an important design implication. Significant ductile response is expected at the flexible edge where ductilities are in conformance with the ductility reduction factor employed in design. Hence, flexible side is mostly responsible for seismic energy dissipation. Although the stiff side may also undergo some inelastic response, particularly when the stiff side strength is close to the flexible side strength (center of strength close to the center of mass), this is quite unexpected in practice. In most practical cases, the *SFSR* is proportional to the ratio of stiff side to flexible side stiffness. This is indeed the cause of torsion as well as the stiff side overstrength, which is a natural consequence. Even the optimal *SFSR*s indicated in Figures 5 and 7 are impossible to achieve, except for low stiffness eccentricities ($e < 0.1$) and low design ductility demands ($R_\mu < 3$). Hence, stiff side performs as a force-controlled system rather than a displacement controlled system with fairly small ductility demands when $SFSR > 2$. This is indeed a very common case in reality. Accordingly, ductile seismic detailing which further increases the overstrength is not consistent for stiff side members.

2.2 | Sensitivity of torsional ductility spectra to uncoupled frequency ratio

The effect of uncoupled frequency ratio is assessed comparatively for uncoupled rotational-to-translational frequency ratios of 1.25, 1.0, and 0.8, representing torsionally stiff, equally stiff, and torsionally flexible systems, respectively. The results are presented in Figure 8 for $R_\mu = 4$; $SFSR = 1.0$, 2.0, and 3.0; and $e = 0.1$, 0.2, and 0.3 combinations.

Apparently, there is a complex interaction among the frequency ratio Ω_r, e, and *SFSR*. Flexible side ductilities for torsionally stiff and equally stiff systems are not affected from Ω_r (1.25 or 1.0) and from the strength ratio *SFSR*. They are very close to R_μ. However, ductility demands for torsionally flexible systems are significantly larger, particularly for smaller stiffness eccentricities ($e < 0.10$) where they reach almost $2R_\mu$.

On the stiff side, ductility demands consistently increase with decreasing frequency ratio. If R_μ is accepted as a threshold value, ductility demands of torsionally flexible systems remain below R_μ only when $SFSR$ 3.0. When *SFSR* is less than 2.0, which is less likely but still a realistic range, ductility demands at the stiff side always exceed R_μ if $e > 0.10$. Hence, there is a reason for discouraging torsionally flexible systems in order to have a better control on inelastic deformation distribution.

2.3 | Sensitivity of torsional ductility spectra to ground motion intensity

Torsional ductility spectra for torsionally stiff and equally stiff systems are also generated for the Maximum Considered Earthquake (MCE) level ground motions, which are identical to the design ground motions in frequency content but scaled by 3/2. Sensitivity to intensity is investigated for $R_\mu = 4$ and $e = 0.2$. All other parameters are the same. The comparative results are shown in Figure 9. Similar ductility increases have been observed on both sides, about 1.6–2.0 times that of DBE ductility demands for all *SFSR* values. This ratio is practically not too different but always larger from the intensity-scaling ratio of 3/2.

3 | IMPLEMENTATION OF TDS TO STRUCTURAL FRAMES

TDS are first implemented to a single-story shear frame with four resisting members by following a direct procedure for transforming a "four-member" system into a parametric 2DOF, two-member system. Although this is an academic case, it is instructive for explaining the key points. Then, the procedure is elaborated on a three-story concrete frame with significant plan asymmetry, by introducing a surrogate modeling approach.

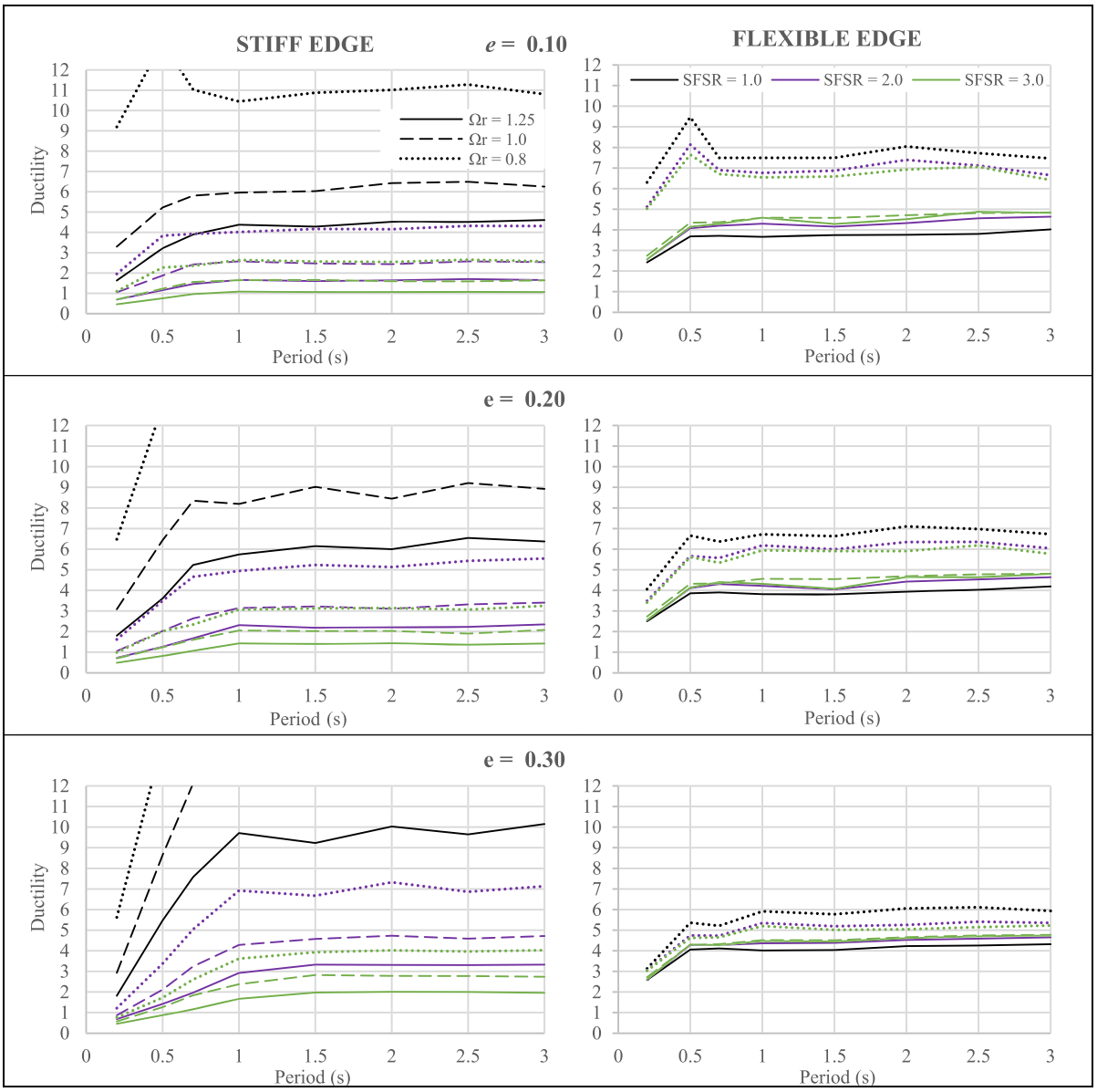

FIGURE 8 Sensitivity of torsional ductility spectra to uncoupled frequency ratio ($R_\mu = 4$) [Colour figure can be viewed at wileyonlinelibrary.com]

3.1 | Single-story shear frame: Direct implementation

The plan view of a shear frame with four members (four-member system) is shown in Figure 10A. It is supporting a rigid slab of length 18 m and width 11.5 m, with a uniform mass of 340 tons. Member 1 has a lateral stiffness of 24 000 kN/m whereas the stiffnesses of the other three members are all 6500 kN/m. These properties lead to the stiffness eccentricity $e = 0.2$, uncoupled frequency ratio $\Omega_r = 1.25$, and modal vibration periods of $T_1 = 0.7$ s, $T_2 = 0.4$ s ($\omega_1^2 = 80.6, \omega_2^2 = 245.5$, both r^2/s^2). This system is designed under the design spectrum in Figure 2 for $R \equiv R_\mu = 4$. Hence, overstrength is dismissed for all members. The resulting strength demands and yield displacements are marked in Figure 10B. The basic objective here is representing the four-member system in Figure 10A with the parametric system in Figure 1A, which was utilized for developing TDSs. The representation is based on an identical set of (T_1, Ω_r, e, R_μ, *SFSR*) values assigned as above except *SFSR*, which will be defined below. Accordingly, it is expected that stiff and flexible side mean maximum ductility ratios obtained under the set of spectrum compatible ground motions from nonlinear response history analysis (NRHA) of the four-member system can be predicted by the associated TDSs in Figure 4.

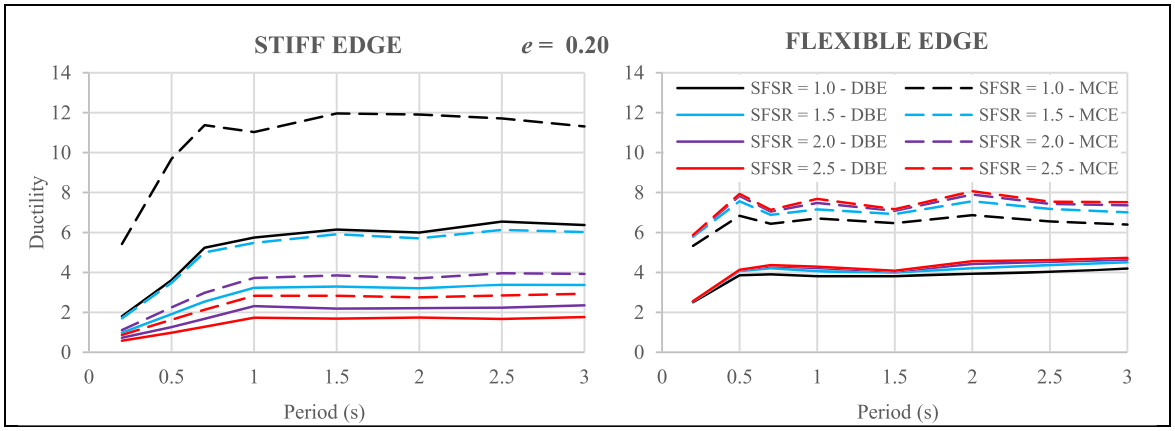

FIGURE 9 Sensitivity of torsional ductility spectra to ground motion intensity ($R_\mu = 4$, $e = 0.20$) [Colour figure can be viewed at wileyonlinelibrary.com]

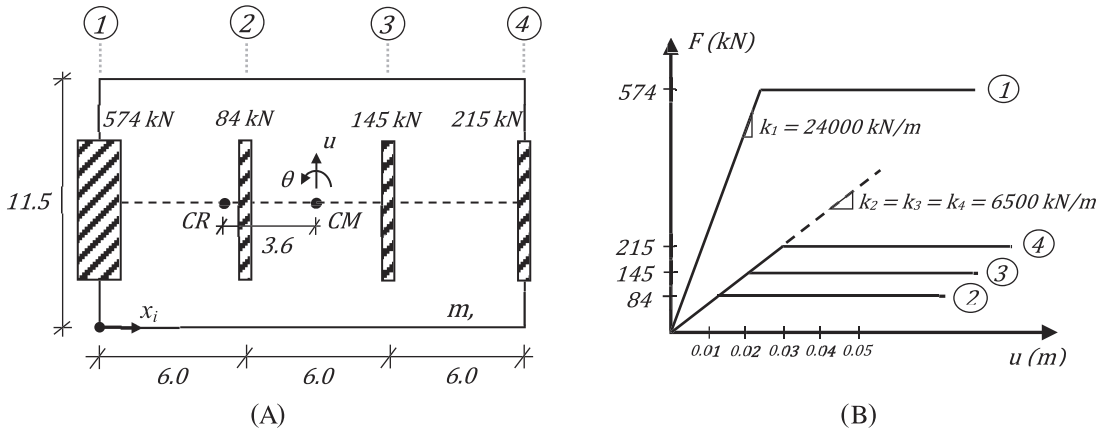

FIGURE 10 A, Four-member single-story frame and B, force–displacement properties of members

Transformation of the strength capacities of four members F_i in Figure 10 to stiff and flexible side strength capacities of the parametric system F_S and F_F in Figure 1 can be simply achieved by satisfying the two equations of equilibrium in Equation 7 where x_i is the location of frame i in the four-member system.

$$F_F = \frac{\sum_i (F_i \cdot x_i)}{L}; F_S = \left(\sum_i F_i\right) - F_F. \tag{7}$$

Equation 7 gives $F_F = 340$ kN and $F_S = 678$ kN. Accordingly, $SFSR = 2.0$. Then, utilizing TDSs in Figure 4 with ($T_1 = 0.7$ s, $\Omega_r = 1.25$, $e = 0.2$, $R_\mu = 4$, $SFSR = 2.0$) provides the expected ductilities for the parametric system, which are $\mu_S = 1.7$; $\mu_F = 4.3$. It should be noted here that the correspondence between the four-member system and the two-member parametric system is not exact because their second mode periods are not identical. T_2 is 0.40 s for the four-member system and 0.43 s for the two-member parametric system. A perfect match is usually not possible. This difference however does not introduce notable error.

Mean maximum inelastic member displacements obtained from NRHA conducted in OpenSees[38] for the four-member system are presented in vector form in Equation 8, along with the yield displacements defined in Figure 10B. Then, the ductility ratios for each member from both analyses are calculated and given in Equation 9. Mean member ductilities calculated by NRHA are seemingly very close to the ductilities directly obtained from the torsional response spectra (*TRS*). Members 2–4 are all on the flexible side of the four-member system. Hence, $\mu_F = 4.3$ is directly applicable to all these members.

An important point must be noted here. Identical ductility reduction factors are imposed to all four members in determining their strengths. However, ductility response of the stiff side member is obtained much lower than the other flexible side members, which achieve ductility ratios close to $R_\mu = 4$. In design practice, larger overstrength is expected to develop at the stiff side members compared with the others, which will further increase the ductility imbalance.

$$\underline{u_i} = \begin{Bmatrix} u_1 \\ u_2 \\ u_3 \\ u_4 \end{Bmatrix} \; ; \; \underline{u}_{NRHA} = \begin{Bmatrix} 0.039 \\ 0.055 \\ 0.096 \\ 0.145 \end{Bmatrix} \; ; \; \underline{u}_y = \begin{Bmatrix} 0.0241 \\ 0.0129 \\ 0.0224 \\ 0.0331 \end{Bmatrix}, \tag{8}$$

$$\mu_{TRS} = \begin{Bmatrix} 1.7 \\ 4.3 \\ 4.3 \\ 4.3 \end{Bmatrix} ; \; \mu_{NRHA} = \begin{Bmatrix} 1.6 \\ 4.3 \\ 4.3 \\ 4.4 \end{Bmatrix}. \tag{9}$$

3.2 | Multistory frame structure: Surrogate model

Although direct implementation of TDS gives a perfect match with NRHA for the four-member system, such a special case would be misleading for generalizing this outcome. In realistic frame structures, lateral stiffnesses and base shear capacities of individual frames cannot be determined directly. Hence, e, R_μ, and *SFSR* are not readily available. A simple procedure is developed herein for transforming the vibration and strength characteristics of multistory moment frames to two-member system parameters. Surrogate models of actual MDOF multistory frames simulate their dynamic response with a 2DOF single-story system, similar to the shear frame shown in Figure 1A.

The characteristic equation (Equation 3) provides a set of two homogeneous equations for solving the modal frequencies ω_1 and ω_2 of a 2DOF asymmetrical system with the stiffness and mass properties defined in Equation 2. This equation can be rearranged for the given values of ω_1 and ω_2 of a 2DOF system where the stiffness coefficients are now unknowns. Its solution leads to another quadratic equation in terms of the stiffness coefficients k. Simplifying the simultaneous solution and introducing Equation 4, a new, transformed characteristic equation is obtained.

$$k^2 - k\frac{m\left(\omega_1^2 + \omega_2^2\right)}{\left(1 + \Omega_r^2\right)} + \left(\frac{m\omega_1\omega_2}{2\Omega_r}\right)^2 = 0. \tag{10}$$

Two roots of the quadratic Equation 10 are k_S and k_F of the 2DOF surrogate model with stiffness and mass properties represented by Equation 2. Similarly, surrogate model of an actual multistory, MDOF asymmetric frame structure can be established in each orthogonal direction by utilizing its lowest translation and rotational modal frequencies, total mass, and the uncoupled frequency ratio. Then, once the stiff and flexible side strength capacities are determined by Equation 7, the surrogate model approximately represents the basic inelastic response characteristics of an actual structure by a single-story shear frame, with a stiff and flexible side inelastic member.

Direct use of Equation 7 is not possible however. Frame base shear capacities F_i of the actual structure are required. Nonlinear static procedures are not warranted for predicting frame base shear capacities because the basic objective of the presented study is avoiding rigorous nonlinear response analysis. An approximate procedure is developed here for calculating frame shear capacities from the already available modal response spectrum analysis results and member design data. Finally, the actual asymmetrical frame structure is transformed to the two-member parametric system through its surrogate model. It should be noted here that each frame in the actual structure is considered as an inelastic shear-resisting member with an associated stiffness and strength.

The proposed procedure is implemented on a three-story concrete frame in the following section.

4 | EXAMPLE: THREE-STORY CONCRETE FRAME

Plan view of the concrete frame is shown in Figure 11. Story heights are 3 m, and member dimensions are constant at all stories. Cross-section dimension are (0.30 × 1.50) m for columns A2 and A3, (0.60 × 0.60) m for column B2, (0.50 × 0.50) m for the other seven columns, and (0.30 × 0.55) m for all beams. The frame is designed according to[1] ASCE 7 and Turkish Earthquake Code[39] regulations under gravity loads and the design spectrum given in Figure 2A by employing a response reduction factor of $R = 8$.

Floor mass m is 183 tons, and mass moment of inertia about the center of mass I_{CM} is 19 625 ton/m^2 at each story. Radius of gyration is 10.35 m accordingly. Center of mass CM is marked on Figure 11. The lowest three modal frequencies (periods) with cracked section inertia are 9.21, 11.26, and 12.90 r/s (0.68, 0.56, and 0.49 s, respectively). The associated three effective modal masses account for 9%, 55%, and 12% of the total mass in the X direction and 34%, 20%, and 23% in the Y direction.

Translational stiffness and rotational stiffness about the center of mass at the first story are calculated by the approximate procedure defined in Eurocode 8 in order to define the uncoupled rotational and translational frequencies.[2] Column lateral stiffnesses are estimated by proportioning with respect to the moments of inertia of their cross sections. Hence, the proportional translational and rotational stiffnesses are obtained as $k_X = k_Y = 1.62$ m^4 and $k_\theta = 198.5$ m^6, respectively. This procedure yields a torsional radius (square root of the torsional stiffness k_θ to lateral stiffness k_X, k_Y) of 11.07 m in both directions. Furthermore, proportional rotational and translational frequencies of the first floor as well as the uncoupled frequency ratio can be calculated from Equations 11a–11c as

$$\omega_\theta = \sqrt{\frac{k_\theta}{I_{CM}}} \equiv 0.100, \tag{11a}$$

$$\omega_X = \omega_Y = \sqrt{\frac{k_{X;Y}}{m}} \equiv 0.094, \tag{11b}$$

$$\Omega_r = \frac{\omega_\theta}{\omega_{X;Y}} = 1.06. \tag{11c}$$

Although k_X, k_Y, and k_θ and consequently ω_θ, ω_X, and ω_Y calculated from Equations 11a and 11b do not have a consistent physical value, their ratios, that is, torsional radius and Ω_r, are physically consistent because the proportionality constants hidden in Equations 11a and 11b cancel out each other in Equation 11c. It leads to $\Omega_r \approx 1$ for all stories of the three-story frame. This uncoupled frequency ratio indicates that the system is nearly torsionally equally stiff. It should be noted that there is no exact analytical procedure for calculating the uncoupled frequency ratio for realistic frames.

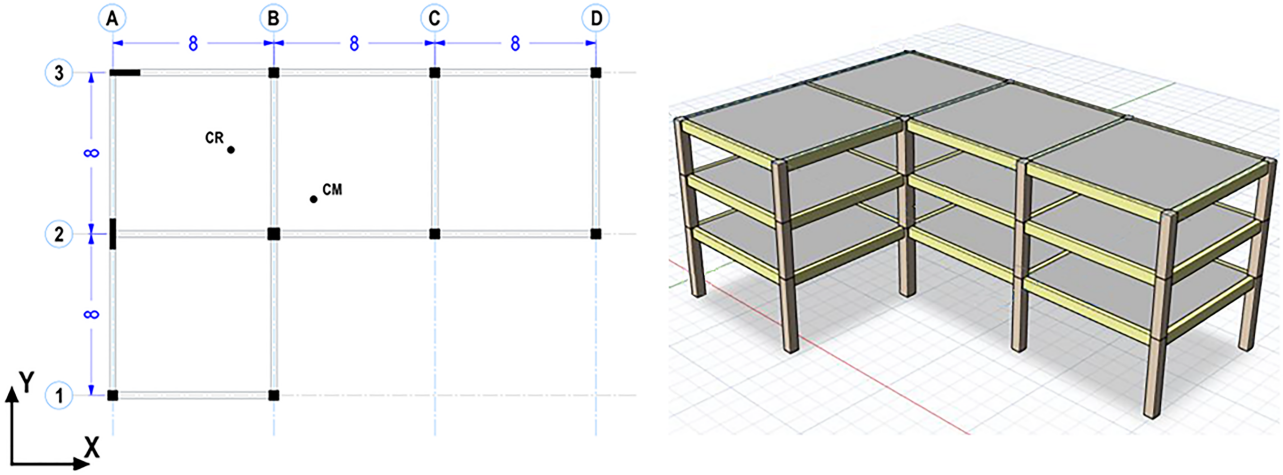

FIGURE 11 Plan view and isometric view of the three-story concrete frame (units in m) [Colour figure can be viewed at wileyonlinelibrary.com]

Seismic design codes employ measures for identifying plan irregularity. Eurocode 8[2] requires two conditions. First, torsional radius should be equal or larger than the radius of gyration at each floor. Torsional radius and radius of gyration were calculated above as 11.07 and 10.35 m, respectively. They are close, but torsional radius is larger. Second, stiffness eccentricity perpendicular to the direction of analysis e_0 should be less than 30% of torsional radius, that is, less than 3.3 m. e_0 cannot be calculated directly for moment frames but can only be estimated by approximate procedures. Eurocode 8 procedure mentioned above leads to $e_{0x} = 4.3$ m for all floors. A more refined procedure developed by Basu and Jain[40] with single floor definition gives $e_{0x} = 3.8$, 3.2, and 2.4 m, respectively, for the first, second, and third floors, corresponding to an eccentricity ratio of 16% at the first story. A similar procedure is also implemented in the ETABS software package. The three-story concrete frame does not satisfy the second condition of Eurocode 8,[2] implying plan irregularity. Response reduction factors are reduced in order to account for plan irregularity in Eurocode 8.

ASCE 7 employs[1] a single control parameter calculated for all floors: δ_{max}/δ_{av}, where δ is the floor displacement, δ_{max} is its maximum value at any point on the floor, and δ_{av} is the average of maximum and minimum displacements at the extreme points. If this ratio is between 1.2 and 1.4, it is considered as "torsional irregularity." Response spectrum analysis is permissible without any modification. When it exceeds 1.4, "extreme torsional irregularity" condition arises that requires amplification of accidental eccentricity. Displacement ratio δ_{max}/δ_{av} is obtained as 1.45, 1.41, and 1.37 for the first, second, and third floors, respectively, from the RSA results. ASCE 7 considers the first floor response as extremely torsionally irregular, confirmed indirectly by the uncoupled frequency ratio $\Omega_r \approx 1$.

4.1 | Construction of surrogate model for the three-story concrete frame

The surrogate model is constructed separately for the X and Y directions. The results are presented in detail for the Y direction with larger eccentricity and summarized for the X direction for brevity.

Equation 10 is solved for the Y direction by employing the three-story frame dynamic parameters, $\omega_1 = 9.2$ r/s (Y-translation dominant first mode), $\omega_2 = 12.9$ r/s (rotation dominant third mode), $m = 549$ tons (total mass), and $\Omega_r = 1.06$, for determining the two side member stiffnesses k_S and k_F of the surrogate model. Solution yields $k_S = 42\,688$ kN/m and $k_F = 22\,030$ kN/m. The corresponding natural frequencies of the surrogate system, obtained by solving Equation 3 are 9.5 and 13.6 r/s. They are very close but slightly higher than the associated frequencies of the actual system. The difference is due to the inability of the single-story, 2DOF surrogate model in representing the inertia distribution of the actual multistory structure that possesses more than 2DOFs, 6 in this particular case.

Center of stiffness of the surrogate Y model with k_S and k_F at the two sides is 8.2 m from the stiff side while the center of mass is at the middle. Hence, $e_x = 3.8$ m and $e_x/L = 15.8\%$. This ratio is sufficiently close to 16% obtained by the Basu–Jain procedure referred above.

The final step in constructing the surrogate model is determining stiff and flexible side member strengths for both directions from Equation 7 in which frame base shear capacities F_i are required. They are not readily available as in the previous four-member case. Nevertheless, they can be determined with sufficient accuracy by using the RSA analysis results and member design forces produced in a new design. Bottom end moment M_{bi} and shear force V_{bi} of the ith column at the ground story of each frame are calculated by modal RSA in design analysis. Moment capacity M_{yi} at the bottom of ith column is also known either from moment-curvature analysis or directly from yield moment equations. Then, M_{bi}/M_{yi} can serve as the response reduction factor for the ith column. If this reduction factor is applied to the linear elastic shear force V_{bi}, and reduced column shears are added for all columns i in a frame, base shear capacity of each frame can be estimated. This procedure is based on the assumption that yielding in lateral load-resisting vertical members of the frames occurs only at their fixed bases, which fully complies with the basic principles of capacity design. All of these operations are collected in Equation 12, where NC is the number of lateral load carrying members in a frame.

$$V_{b,\ Frame} = \sum_{i=1}^{NC} V_{bi}\left(\frac{M_{yi}}{M_{bi}}\right). \tag{12}$$

Equation 12 is applied to the first story columns of the three-story concrete frame and presented in a tabular form in Table 1 for Y direction. Moment-curvature diagrams of the first story column bottom ends are given in Figure 12.

Frame shear capacities calculated in Table 1 are substituted into Equation 7, and the capacities of stiff and flexible side members of the surrogate Y model are obtained as $F_S = 910$ kN and $F_F = 493$ kN. Accordingly, $SFSR = 1.85$.

TABLE 1 Frame base shear capacities—*Y* direction

Frame ID	Frame A			Frame B			Frame C		Frame D	
Column ID	A1	A2	A3	B1	B2	B3	C1	C2	D1	D2
V_b (kN): RSA	103	1002	79	138	279	138	221	221	317	317
M_b (kN/m): RSA	340	4633	233	424	871	424	658	658	936	936
M_y (kN/m): M-ϕ	310	1740	280	300	640	300	350	350	300	300
$R_\mu = M_b/M_y$	1.10	2.66	0.83	1.41	1.36	1.41	1.88	1.88	3.12	3.12
$V_{b,Frame}$ (kN)	565			400			235		203	

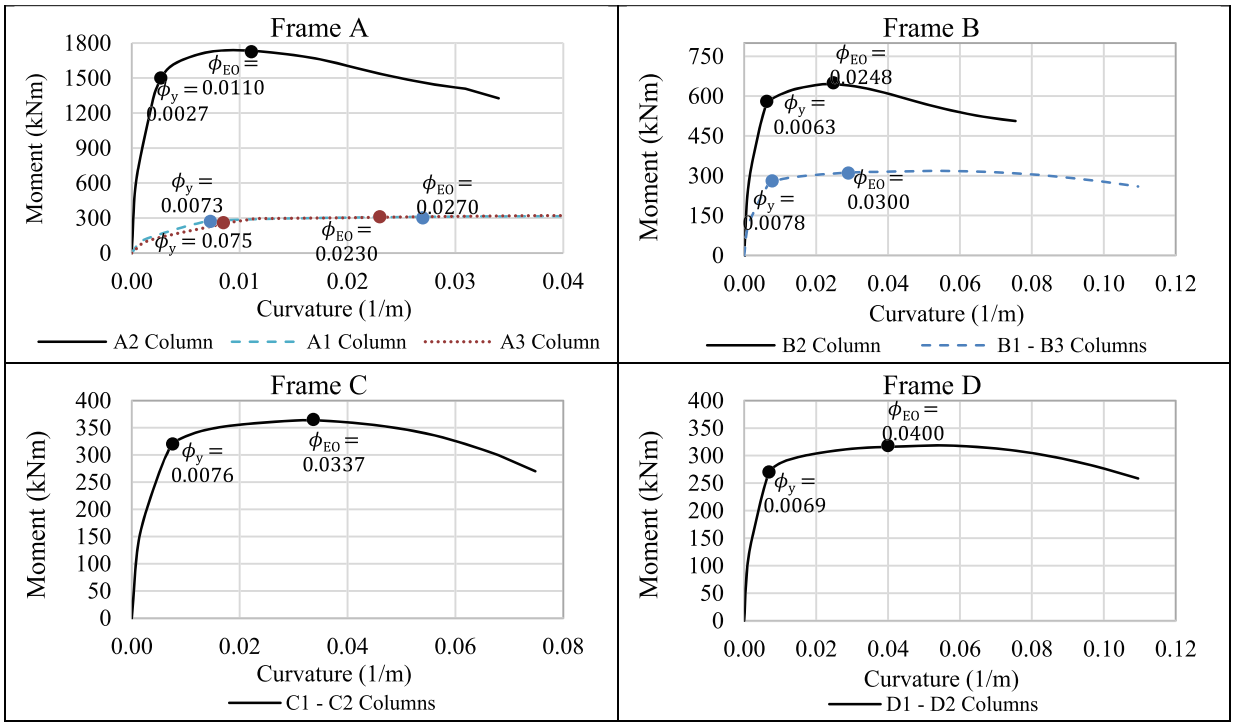

FIGURE 12 Moment-curvature diagrams of column bottom ends at the ground story [Colour figure can be viewed at wileyonlinelibrary.com]

The surrogate model constructed for the three-story concrete frame in the *Y* direction and modal displacements calculated by RSA are shown in Figure 13. Analytical expressions for mode shapes and modal parameters required in RSA are presented in Appendix B.

Finally, ductility reduction factor for the flexible side member of the surrogate model is calculated for accessing the TDSs. By definition, it is the elastic strength demand divided by strength capacity, that is, 493 kN. Elastic strength demand at the flexible side F_{Fe} is the product of flexible edge stiffness $k_F = 22\,030$ kN/m and elastic displacement of the flexible side. Modal RSA for the 2DOF surrogate model under design spectrum in Figure 2A yields $u_S = 0.0459$ m and $u_F = 0.1127$ m. Both of these values can be obtained by hand computation by using the closed-form analytical expressions given in Appendix B. Accordingly, ductility reduction factor at the flexible side is calculated as $R_\mu = 5.04$.

Stiff and flexible side ductility ratios are then obtained from the TDS charts for the set of five surrogate model parameters: ($T = 0.66$ s, $e_x/L = 0.16$, $\Omega_r = 1$, $SFSR = 1.85$, $R_\mu = 5$). Spectral charts in Figures 3–10 are not available for $e = 0.16$ but interpolation is acceptable. Interpolating between ($R_\mu = 5$, $e = 0.10$) and ($R_\mu = 5$, $e = 0.20$) with $SFSR = 1.85$ in Figure 6 gives $\mu_S = 4.0$ and $\mu_F = 5.7$.

The corresponding values for the surrogate *X* model are $\Omega_r = 1$, $k_S = 42\,306$ kN/m, $k_F = 33\,204$ kN/m, $T = 0.71$ s, $e_y/L = 6\%$, $F_S = 963$ kN, $F_F = 465$ kN ($SFSR = 2.07$), and $R_\mu = 4.1$. Extrapolating from ($R_\mu = 4$, $e = 0.20$) to ($R_\mu = 4$, $e = 0.10$) for $e = 0.06$ with $SFSR = 2.0$ in Figure 4 gives $\mu_S = 2.8$ and $\mu_F = 4.3$.

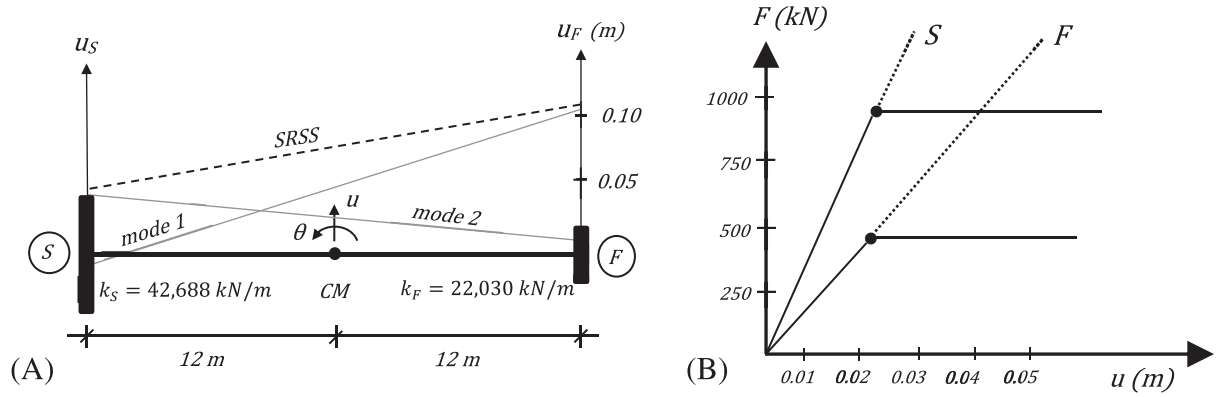

FIGURE 13 Surrogate model for three-story concrete frame. A, Model parameters and RSA results ($\omega_1 = 9.5$ r/s, $\omega_2 = 13.6$ r/s, $\Omega_r = 1.06$, $L = 24$ m, $m = 549$ tons) and B, force–displacement relations of stiff and flexible side members

TABLE 2 Curvature and rotation ductilities at the fixed bases of vertical members (NRHA): *Y* direction

Frame ID	Frame A			Frame B			Frame C		Frame D	
Column ID	A1	A2	A3	B1	B2	B3	C1	C2	D1	D2
Curvatures										
ϕ_y (1/m)	0.0073	0.0027	0.0075	0.0078	0.0063	0.0078	0.0076	0.0076	0.0069	0.0069
ϕ_{NRHA} (1/m)	0.0270	0.0111	0.0230	0.0300	0.0248	0.0286	0.0337	0.0334	0.0400	0.0401
μ_ϕ (NRHA)	**3.7**	**4.1**	**3.1**	**3.8**	**3.9**	**3.7**	**4.4**	**4.4**	**5.8**	**5.8**
Rotations										
θ_y (rad)	0.0022	0.0024	0.0020	0.0023	0.0023	0.0023	0.0023	0.0023	0.0021	0.0021
θ_{NRHA} (rad)	0.0087	0.0087	0.0087	0.0093	0.0093	0.0093	0.0105	0.0105	0.0120	0.0120
θ_{RSA} (rad)	0.0033	0.0033	0.0033	0.0040	0.0040	0.0040	0.0061	0.0061	0.0086	0.0086
μ_θ (NRHA)	**3.9**	**3.6**	**4.3**	**4.0**	**4.0**	**4.0**	**4.6**	**4.6**	**5.7**	**5.7**
μ_θ (RSA)	**1.5**	**1.4**	**1.7**	**1.7**	**1.7**	**1.7**	**2.7**	**2.7**	**4.1**	**4.1**

Abbreviation: NRHA, nonlinear response history analysis.

These ductility ratios indicate the ductility performances of the stiff and flexible side frames of the actual three-story concrete frame in *X* and *Y* directions under design ground motions. In asymmetric-plan structures, ductility demands are larger and more critical at the flexible side exterior frames mainly due to larger displacement demands and lower strength supplies ($SFSR > 1$) compared with the stiff side. The first factor is of course a well-known fact in earthquake engineering, but the second one is usually not considered properly.

4.2 | Comparison of spectral ductility demands with NRHA results

The procedure proposed here for estimating the ductility demands of stiff and flexible side frames in asymmetric-plan building structures is tested with the results from NRHA of the three-story building frame. Nonlinear dynamic analyses are conducted with the OpenSees[38] software. Fiber element modeling is adopted for columns along their plastic hinge length, whereas beams are defined with lumped plasticity idealization at their ends involving bilinear moment-curvature properties. Design spectrum compatible ground motions given in Appendix A are used in NRHA. Comparisons are prepared for curvature and chord rotation ductilities at the fixed bases of the first story vertical members.

Mean maximum curvature and chord rotation demands at the fixed bases of vertical members, calculated by NRHA under the set of 30 ground motions in the *Y* direction, are given in Table 2, rows 5 and 9, respectively. Yield curvatures ϕ_y displayed in Table 2 are directly obtained from the moment-curvature diagrams presented in Figure 12, where yield

points are marked on each curve. Although yield points are evident for the column members through visual observation of these curves, it is not quite the case for column A2 cross section having several longitudinal bars along its length l_w. Yield curvature is obtained from the basic principle of mechanics commonly applied to reinforced concrete sections at impending yielding, by assuming that neutral axis is at the centroid. ε_y is the yield strain in Equation 13, equal to 0.002 for steel reinforcement.

$$\phi_{y,w} = \frac{2\,\varepsilon_y}{l_w}. \tag{13}$$

Yield rotations θ_y of column and wall sections given in Table 2 are calculated by the empirical equation (Equation 14) for confined rectangular sections, where $(0.6d)$ is the plastic hinge length l_p and d is the effective section depth.

$$\theta_y = \phi_y \cdot (0.6d). \tag{14}$$

Although assuming $l_p = 0.5d$ is a common practice in reinforced concrete, several empirical equations given in Park and Paulay[41] always give $l_p > 0.6d$, where l_p increases with the shear span to depth ratio of the member. We have decided to use the lower bound value for the plastic hinge length which is still higher than $0.5d$.

Mean curvature and rotation ductility demands obtained from NRHA under Y direction earthquake excitations are presented in Table 2, rows 6 and 11. They are consistent and further suggest that ductility demands estimated by the method proposed herein for the vertical members of stiff and flexible side frames are quite reasonable. Moreover, rotation ductilities are also estimated by employing the chord rotations from RSA. They are presented in the last row of Table 2 for comparison. Such comparison is found necessary, because estimating inelastic deformations from linear elastic analysis results (equal displacement rule) is the only option for the designer for performance assessment, unless a comprehensive nonlinear dynamic analysis is carried out. It is evident that equal displacement rule (RSA) is not as trustworthy as it is in plane frames for estimating inelastic deformations of asymmetric-plan systems.

Chord rotation ductilities for the first story column bottom ends are presented in Figure 14 in graphical form for both Y ($e_x/L = 0.16$) and X ($e_y/L = 0.06$) directions. Ductility values for column ends are averaged for each frame in Figure 14.

Ductility ratios estimated by the TDS at the two exterior sides are sufficiently close to the NRHA results obtained at the first story column ends of these frames. TDS do not account for the effect of gravity loads on column lateral deformations, which is also insignificant in NRHA or RSA as long as the second-order effects are negligible. Hence, TDS results are directly applicable to vertical members that have primarily role in resisting torsion.

5 | SUMMARY

Implementation of the procedure developed for predicting the ductility distribution in asymmetric-plan systems under strong ground motion excitations is summarized here in an algorithmic form.

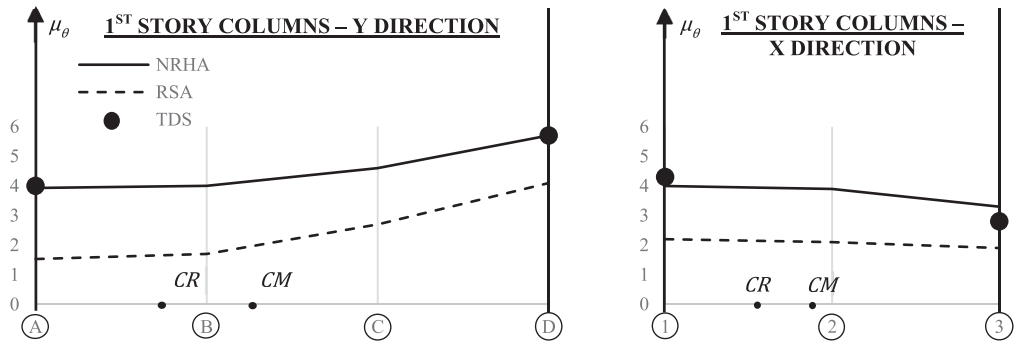

FIGURE 14 Rotation ductility distribution at column bottom ends. A, Y direction and B, X direction

1. Structural Analysis and Design Data of the Building Frame

a. Modal RSA: ω_n, elasic force demands of columns (M_{bi},V_{bi}) at the ground story.
b. Eurocode 8 torsion analysis at the ground story: Classification of torsional stiffness. Torsionally stiff ($\Omega_r > 1$), torsionally equally stiff ($\Omega_r \approx 1$), or torsionally flexible ($\Omega_r < 1$).
c. Capacity design: Moment capacities of column fixed ends (M_{yi}) at the ground story.
d. Equation 12: Frame base shear capacities.

2. Surrogate Model

a. Equation 7: Transformation of frame base shear capacities to stiff and flexible side member capacities of the surrogate model (F_S, F_F).
b. Equation 6: *SFSR*
c. Select Ω_r. 1.25 for torsionally stiff, 1.0 for torsionally equally stiff, 0.8 for torsionally flexible systems.
d. Equation 10: k_S, k_F, and e
e. RSA (Appendix B): Elastic force demand at the flexible side (F_{Fe}).
f. Ductility reduction factor: $R_\mu = \frac{F_{Fe}}{F_F}$

3. Torsional Ductility Spectrum (T_1, e, Ω_r, *SFSR*, R_μ): μ_S and μ_F

6 | CONCLUSIONS

Structural analysis and design data are naturally available for newly designed buildings. The computations listed in the algorithm given above can be carried out with simple hand calculations. Accordingly, implementation of the procedure to an existing building is easy, not an additional burden on the design engineer. Its return however is valuable, effectively informative in assessing the seismic performance of building structure.

Almost all buildings are asymmetrical in reality. Hence, torsional coupling leading to torsional response is inevitable under earthquake excitation. Torsion cannot be eliminated, but the resulting deformation demands can be controlled if they are predicted reasonably well. TDS developed in this study provides estimation of ductility demands in the vertical members of code-designed, regular asymmetric-plan building frames under strong ground motion excitation with acceptable accuracy, without conducting rigorous nonlinear dynamic analysis.

The results obtained from this study further suggest the following conclusions.

- Stiff side frames of torsionally stiff or equally stiff asymmetric systems do not necessarily require high ductility detailing requirements.
- Ductility demands in torsionally flexible systems are significantly larger at both sides compared with torsionally stiff and equally stiff systems.

ORCID

Halûk Sucuoğlu https://orcid.org/0000-0003-4475-8182
Kaan Kaatsız https://orcid.org/0000-0001-9842-3607

REFERENCES

1. American Society of Civil Engineers. Minimum design loads for buildings and other structures (ASCE/SEI 7-16), 2016.
2. European Committee for Standardization. EN 1998-1 Eurocode 8: Design of structures for earthquake resistance, 2004.
3. Rutenberg A. Nonlinear response of asymmetric building structures and seismic codes: A state of the art review. In: Fajfar P, Krawinkler H, eds. *Nonlinear Seismic Analysis and Design of Reinforced Concrete Buildings*. London: Elsevier Publishers; 1992.
4. Anagnostopoulos SA, Alexopoulou C, Stathopoulos K. An answer to an important controversy and the need for caution when using simple models to predict inelastic earthquake response of buildings with torsion. *Earthq Eng Struct Dyn*. 2010;39:521-540.
5. Erdik MO. Torsional effects in dynamically excited structures. Ph.D. Thesis, Rice University, Houston, 1975.

6. Kan CL, Chopra AK. Torsional coupling and earthquake response of simple elastic and inelastic systems. *J Struct Div*. 1981;107:1569-1588.
7. Chandler AM, Hutchinson GL. Torsional coupling effects in the earthquake response of asymmetric buildings. *Eng Struct*. 1986;8(4):222-236.
8. Tso WK, Bozorgnia Y. Effective eccentricity for inelastic response of buildings. *Earthq Eng Struct Dyn*. 1986;14(3):413-427.
9. Rutenberg A, Eisenberger M, Shohet G. Reducing seismic ductility demand in asymmetric shear buildings. Proceedings of the 8th European Conference on Earthquake Engineering, Lisbon, 1986, Vol. 6.7:57–64.
10. Rutenberg A, Eisenberger M, Shohet G. Inelastic seismic response of code designed single storey asymmetric structures. *Eng Struct*. 1992;14(2):91-102.
11. Goel R, Chopra AK. Effects of plan asymmetry in inelastic seismic response of one-story systems. *J Struct Eng*. 1991;117(5):1492-1513.
12. Goel RK, Chopra AK. Dual-level approach for seismic design of asymmetric-plan buildings. *J Struct Eng*. 1994;120(1):161-179.
13. Chandler AM, Duan XN. Performance of asymmetric code-designed buildings for serviceability and ultimate limit states. *Earthq Eng Struct Dyn*. 1997;26(7):717-735.
14. Correnza JC, Hutchinson GL, Chandler AM. Seismic response of flexible-edge elements in code-designed torsionally unbalanced structures. *Eng Struct*. 1995;17:156-166.
15. Paulay T. A behaviour based design approach to earthquake induces torsion. In: Fajfar P, Krawinkler H, eds. *Seismic Methodologies for the Next Generation of Codes*. Rotterdam: Balkema; 1977.
16. Humar JL, Kumar P. A new look at the torsion design provisions in seismic building codes. Proceedings of the 12th World Conference on Earthquake Engineering, Auckland, 2000, Paper No. 1707.
17. Myslimaj B, Tso WK. A design oriented approach to strength distribution in single-story asymmetric systems with elements having strength-dependent stiffness. *Earthq Spectra*. 2005;21(1):197-212.
18. Paulay T. Torsional mechanisms in ductile building systems. *Earthq Eng Struct Dyn*. 1998;27(10):1101-1121.
19. Humar JL, Kumar P. Effect of orthogonal in plane structural elements on inelastic torsional response. *Earthq Eng Struct Dyn*. 1999;28(10):1071-1097.
20. Kaatsız K, Sucuoğlu H. The role of overstrength on the seismic performance of asymmetric-plan structures. *Earthq Eng Struct Dyn*. 2019;48(4):412-431.
21. Rutenberg A. Behaviour or irregular and complex structures asymmetric structures—progress since 1998. Proceedings of the 12th European Conference on Earthquake Engineering, London, 2002; Paper No. 832.
22. De Stefano M, Pintucchi B. A review of research on seismic behavior of irregular structures since 2002. *Bull Earthq Eng*. 2008;6(2):285-308.
23. Anagnostopoulos SA, Krykos MT, Stathopoulos KG. Earthquake induced torsion in buildings: critical review and state of the art. *Earthq Struct*. 2015;121(2):305-377.
24. Stathopoulos KG, Anagnostopoulos SA. Accidental design eccentricity: is it important for the inelastic response of buildings to strong earthquakes? *Soil Dyn Earthq Eng*. 2010;30(9):782-797.
25. Duan XN, Chandler AM. Inelastic seismic response of code-designed multistory frame buildings with regular asymmetry. *Earthq Eng Struct Dyn*. 1993;22(5):431-445.
26. De La Llera JC, Chopra AK. Inelastic behavior of asymmetric multistory buildings. *J Struct Eng*. 1996;122(6):597-606.
27. Lee SL, Hwang KR. Torsion design implications from shake-table responses of an RC low-rise building model having irregularities at the ground story. *Earthq Eng Struct Dyn*. 2015;44(6):907-927.
28. Marusic D, Fajfar P. On the inelastic seismic response of asymmetric buildings under bi-axial excitation. *Earthq Eng Struct Dyn*. 2005;34:943-963.
29. Stathopoulos KG, Anagnostopoulos SA. Inelastic torsion of multistory buildings under earthquake excitations. *Earthq Eng Struct Dyn*. 2005;34(12):1449-1465.
30. Kyrkos MT, Anagnostopoulos SA. Improved earthquake resistant design of torsionally stiff asymmetric steel buildings. *Earthq Struct*. 2011;2(2):127-147.
31. Kyrkos MT, Anagnostopoulos SA. Improved earthquake resistant design of eccentric steel buildings. *Soil Dyn Earthq Eng*. 2013;47:144-156.
32. De Stefano M, Marino EM, Rossi PP. Effect of overstrength on the seismic behaviour of multi-Storey regularly asymmetric buildings. *Bull Earthq Eng*. 2006;4(1):23-42.
33. Ghersi A, Marino EM, Rossi PP. Static versus modal analysis: influence on inelastic response of multi-story asymmetric buildings. *Bull Earthq Eng*. 2007;5(4):511-532.
34. Kosmopoulos AJ, Fardis MN. Estimation of inelastic seismic deformations in asymmetric multistory RC buildings. *Earthq Eng Struct Dyn*. 2007;36(9):1209-1234.
35. Bahmani P, van de Lindt JW, Dao TN. Displacement-based design of buildings with torsion: theory and verification. *J Struct Eng*. 2014;140(6):401-420, 04014020.
36. PEER Ground Motion Database. Available from: http://ngawest2.berkeley.edu, 2019.
37. Hancock J, Watson-Lamprey J, Abrahamson NA, et al. Improved method of matching response spectra of recorded earthquake ground motion using wavelets. *J Earthq Eng*. 2006;10(sup001):67-89.
38. Open System for Earthquake Engineering Simulation. Available from: http://opensees.berkeley.edu, 2019.

39. Disaster and Emergency Management Directorate, AFAD. Turkish Earthquake Code for building structures: specifications for design of buildings under earthquake forces, Ankara, Turkey, 2018.
40. Basu D, Jain SK. Alternative method to locate center of rigidity in asymmetric buildings. *Earthq Eng Struct Dyn*. 2007;36(7):965-973.
41. Park R, Paulay T. *Reinforced Concrete Structures*. New York: John Wiley and Sons; 1975.

How to cite this article: Sucuoğlu H, Kaatsız K. Torsional ductility spectrum for predicting ductility distribution in simple asymmetric-plan structures. *Earthquake Engng Struct Dyn*. 2021;50:538–559. https://doi.org/10.1002/eqe.3345

APPENDIX A: SEISMOLOGICAL PROPERTIES OF STRONG GROUND MOTIONS

PEER NGA code	Earthquake	M_W	Joyner–Boore dist. (km)	NEHRP site class	PGA (g)
TMB205	Parkfield—1966	6.19	15.96	C	0.29
UC2090	Loma Prieta—1989	6.93	12.15	C	0.34
WPI046	Northridge—01-1994	6.69	2.11	D	0.38
A-TAR000	Whittier Narrows—01-1987	5.99	38.24	D	0.60
ABBAR–L	Manjil, Iran—1990	7.37	12.56	C	0.51
AND250	Morgan Hill—1984	6.19	3.22	C	0.34
B-PTS225	Superstition Hills—02-1987	6.54	0.95	D	0.45
C05085	Parkfield—966	6.19	9.58	D	0.38
CPE045	Victoria, Mexico—1980	6.33	13.80	C	0.57
375-E	Duzce, Turkey—1999	7.14	3.93	C	0.74
DAY-LN	Tabas, Iran—1978	7.35	20.63[a]	C	0.35
DZC270	Kocaeli, Turkey—1999	7.51	13.60	D	0.33
G02090	Loma Prieta—1989	6.93	10.38	D	0.35
G03090	Loma Prieta—1989	6.93	12.23	D	0.46
H-E07230	Imperial Valley—06-1979	6.53	0.56	D	0.42
H-E08230	Imperial Valley—06-1979	6.53	3.86	D	0.54
HEC090	Hector Mine—1999	7.13	10.35	C	0.31
KAK090	Kobe, Japan—1995	6.90	22.50	D	0.27
LGP090	Loma Prieta—1989	6.93	18.46[a]	C	0.78
LOB000	Loma Prieta—1989	6.93	12.04	C	0.46
MU2035	Northridge—01-1994	6.69	12.39	C	0.51
NWH360	Northridge—01-1994	6.69	3.16	D	0.70
OBR360	Northridge—01-1994	6.69	35.43	D	0.47
ORR360	Northridge—01-1994	6.69	20.10	C	0.49
PAR--T	Northridge—01-1994	6.69	5.54	D	0.51
A-MAT353	New Zealand—03-1987	5.80	26.85[a]	C	0.05
STG000	Loma Prieta—1989	6.93	7.58	C	0.38
STM360	Northridge—01-1994	6.69	17.28	D	0.59
STN110	Whittier Narrows—01-1987	5.99	20.35	D	0.12
SYL090	Whittier Narrows—01-1987	5.99	38.55	C	0.06

[a] Epicenter distances are given rather than the Joyner–Boore distances for the marked strong ground motion records.

APPENDIX B: MODAL EXPRESSIONS FOR THE SURROGATE MODEL

$$\underline{\varphi}_n^T = \left\{1,\ \frac{2\left(k_S + k_F - \omega_n^2 m\right)}{L\left(k_S - k_F\right)}\right\}; L_n = m;\ M_n = m\left[1 + \frac{\left(k_S + k_F - \omega_n^2 m\right)^2}{\Omega_r^2 \left(k_S - k_F\right)^2}\right],$$

$$\underline{u}_n \equiv \begin{Bmatrix} u_n \\ \theta_n \end{Bmatrix} = \frac{L_n}{M_n}\frac{A_n}{\omega_n^2}\underline{\varphi}_n^T;\ \underline{f}_n \equiv \begin{Bmatrix} F_n \\ T_n \end{Bmatrix} = \frac{L_n}{M_n}\frac{A_n}{\omega_n^2}\omega_n^2 \underline{m}\,\underline{\varphi}_n^T; \underline{m} = m\begin{bmatrix} 1 & 0 \\ 0 & \dfrac{L^2}{4\Omega_r^2} \end{bmatrix}; A_n : \text{Modal spectral acceleration},$$

$$u_{S,n} = u_n - \frac{L}{2}\theta_n \ ;\quad u_{F,n} = u_n + \frac{L}{2}\theta_n;\ F_{S,n} = \frac{L}{2}F_n - T_n \ ;\quad F_{F,n} = \frac{L}{2}F_n + T_n, n = 1,2.$$